ARTICLE TYPE

Graphene mechanics: I. Efficient first principles based Morse potential[†]

Bogdan I. Costescu,[a] **Ilona B. Baldus,**[a] **and Frauke Gräter**[ab*]

We present a computationally efficient pairwise potential for use in molecular dynamics simulations of large graphene or carbon nanotube systems, in particular those under mechanical deformation, and also for mixed systems including biomolecules. Based on the Morse potential, it is only slightly more complex and computationally expensive than a harmonic bond potential, allowing such large or mixed simulations to reach experimentally relevant time scales. By fitting to data obtained from quantum mechanics (QM) calculations to represent bond breaking in graphene patches, we obtain a dissociation energy of 805 kJ mol^{-1} which reflects the steepness of the QM potential up to the inflection point. A distinctive feature of our potential is its truncation at the inflection point, allowing a realistic treatment of ruptured C-C bonds without relying on a bond order model. Results obtained from equilibrium MD simulations using our potential compare favorably with results obtained from experiments and from similar simulations with more complex and computationally expensive potentials.

1 Introduction

Due to their favorable physical properties, graphene sheets and carbon nanotubes (CNTs) have attracted considerable interest, leading to a large body of theoretical and experimental results. For theoretical studies of these highly conjugated π-systems at atomistic level, quantum mechanics (QM) calculations, classical Molecular Dynamics (MD) simulations or coupled quantum mechanical/molecular mechanical (QM/MM) calculations have been used. QM-based methods take the electronic degrees of freedom into account, and therefore allow considering electronic delocalization, electronic excitation, and optical properties[1,2]. However, for large scale simulations involving more than a few thousands atoms, QM calculations become computationally too expensive, even if tight-binding methods are applied. On the contrary, MD calculations can easily scale to millions of atoms, allowing simulations of molecular systems that reach experimental length scales.

For MD simulations of graphene and CNTs, many potentials have been proposed[3–10], most of which are based on multi-body interactions. These potentials have been developed, applied and improved over decades, and in various studies have proven to model well properties of graphene and

CNTs. Lately, there is a growing interest in MD simulations mixing graphene and CNTs with biomolecules[11–14]. Such simulations would combine a force field specific to carbon compounds (like AIREBO[7]) with a biomolecular one, or use a force field which is able to describe both components (like ReaxFF[9]). Both AIREBO and ReaxFF use the concept of bond order, which correctly takes into account changes in the electron delocalization, an important feature of the aromatic graphene or CNT systems. However, the usage of bond order potentials leads to several disadvantages with regard to efficiency and implementation. One of them is a small integration time step (0.1–0.5 fs) which is needed to handle smooth transitions between the different hybridization states; by contrast, harmonic potentials used in biomolecular force fields allow a time step of 1–4 fs, making possible simulations on biologically relevant time scales. A mixed simulation would need to use the smaller of the two time steps and make the simulation significantly more computationally demanding, unless a multiple time step scheme is used. Another disadvantage of a bond order potential is that any pair of atoms can become bond partners and an atomic neighbor search has to be performed at each time step; by contrast, a biomolecular force field is typically used with a list of bonds built only once, at the start of the simulation. The neighbor search can take a significant percentage of the overall computation time and is much more complex to implement than a list of bonds. For these reasons, the software packages typically used for biomolecular simulations[15–17] avoid implementing bond order potentials and use mainly pairwise potentials. Bond order potentials are implemented mostly in software packages used for materials

research, which either do not include biomolecular force fields or lack validation when used with them. Hence, a pairwise bond potential for graphene and CNTs would be desirable for efficient simulations bringing together carbon based and biomolecular components, opening a simple avenue for mixed simulations including graphene or CNTs to the biosimulation community. The aim of our work is the development of such a potential, striking a good compromise between reproducing several important mechanical properties of graphene and having a high computational efficiency and low implementation complexity.

Biomolecules or assemblies of them are soft and interact weakly with graphene and CNTs under ambient conditions. As a consequence, the bonds in these carbon based compounds are not stretched far away from their equilibrium bond length and a simple pairwise harmonic bond potential describes their elongations well. Away from ambient conditions (like higher pressure) or when mechanical stress can produce significant deformations of the graphene sheets or CNTs, C-C bonds can elongate far from their equilibrium bond length and even break, both of which are not well represented by a harmonic bond potential. A more realistic model for such situations uses the Morse potential, a pairwise potential already used to represent C-C interactions in graphene and CNTs [3]. The Morse potential is already implemented in GROMACS and can be straightforwardly implemented in other MD packages for biomolecules. It is only slightly more computationally expensive than a harmonic bond potential and at the same time is able to correctly reproduce the energy convergence toward the dissociation energy upon stretching, making it suitable to model bond breaking. Building on these advantages, we here introduce a simple modification of the Morse potential which allows monitoring bond breaking in graphene and we parametrize it by fitting to high level quantum mechanical calculations on graphene patches. In addition, we compare mechanical properties of our model with those obtained from experiments or from MD simulations with a more complex potential. Finally, we show that our potential is significantly more computationally efficient than other reactive force fields used to model carbon based compounds.

2   A truncated Morse potential

In MD simulations, the harmonic potential, typically used in proteins to model bonds between atoms, cannot represent bond breaking, as the attractive force increases linearly with the distance between atoms. The more complex potentials derived for carbon structures are so-called bond order potentials which correlate the hybridization of the carbon atom with bond strength, also allowing them to model bond breaking. However, they need to take into account not only the bond but also its environment, including in some cases long-range in-
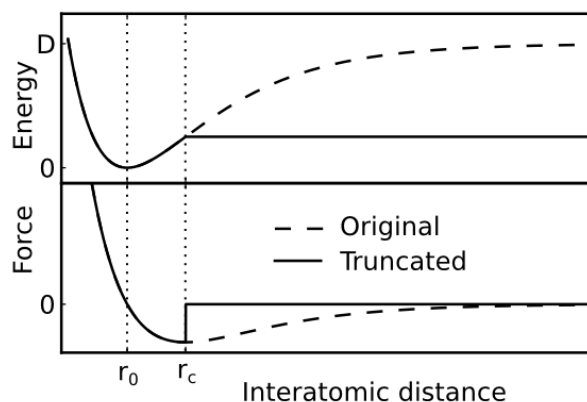
Fig. 1 The variation of energy and force with respect to the interatomic distance for the original (dashed line) and truncated (solid line) Morse potentials. r_0 represents the equilibrium bond length, r_c represents the critical bond length, and D is the dissociation energy.

teractions [8]. Thus, these potentials are computationally much more demanding and mostly incompatible with biomolecular force fields and MD packages.

The Morse potential has often been used to model bond breaking because, at large bond elongations, the attractive force decreases exponentially towards zero. Its applicability to fracture of graphene and CNTs has been investigated by Belytschko et al. [3] which concluded that, for small initial defects, the inflection point of the potential and much less the dissociation energy determines the fracture strength.

We can define the bond length at the inflection point of the Morse potential, corresponding to the maximum of the attractive force, to be the critical bond length, r_c, where the bond resists the most to rupture; for any length greater than this, the bond can be considered broken. However, for a bond stretched far beyond the critical bond length, the Morse potential has a non-zero restoring force that causes unrealistic bond reformation. To prevent bonds from reforming, we introduce a modification to the Morse potential: for bond lengths lower than or equal to r_c, it retains the form of the original Morse potential, while for bond lengths higher than r_c the potential remains constant, retaining its value at r_c, which translates into a zero force (Fig. 1). As a consequence, a bond elongated beyond its critical length is unable to converge on its own towards the equilibrium bond length. Only if the stress which leads to the bond elongation is reduced or removed, thermal fluctuations or other potentials could act on the two atoms connected by the bond, bringing them closer than the critical bond length and leading to a reforming of the bond. Unrealistic reformation of bonds stretched to several nanometers is thereby avoided. When a bond crosses its critical length, our implementation of this potential reports the bond as broken and can optionally

stop the MD simulation. Its obvious limitation is the inability to simulate bond reforming between different carbon atoms or between carbon atoms and other atomic species without major code modifications in MD software packages; if such reaction mechanisms are expected, a slower, more complex bond order potential (like AIREBO or ReaxFF) should be used instead.

The form of the Morse potential between atoms i and j, as implemented in GROMACS, is:

$$V_{\text{Morse}}(r_{ij}) = D_{ij}[1 - e^{-\beta_{ij}(r_{ij}-bij)}]^2 \qquad (1)$$

where D_{ij} is the dissociation energy, β_{ij} is a constant defining the steepness of the energy well and b_{ij} is the equilibrium distance; β_{ij} can be derived from the force constant for the harmonic bond potential and D_{ij}[18]. As the OPLS-AA force field has already been parametrized for groups which include aromatic rings, we use the force constant and the equilibrium length for an aromatic C-C bond (392459.2 kJ mol^{-1} nm^{-2} and 0.140 nm, respectively).

D_{ij} is typically obtained from experimental data or QM calculations. Belytschko et al.[3] use a value of 518 kJ mol^{-1}, the same mentioned by Atkins[19]; GROMACS includes a value of 480 kJ mol^{-1}. Other systems of conjugated double bonds have similar dissociation energies, namely 485 kJ mol^{-1} for vinyl-vinyl and phenyl-vinyl and 493 kJ mol^{-1} for phenyl-phenyl[20]. These values usually model the elongation of an individual bond, showing the variation of one bond potential with the inter-atomic distance while keeping constant all other interactions. Such a situation is impossible in graphene, given its network of identical bonds. We therefore use a two-step approach for calculating D_{ij}: gradually shifting a set of C atoms out of the graphene plane in QM calculations and using the obtained energy profiles as reference to fit MM calculations, where D_{ij} acts as the fitting parameter.

The graphene patches and sets of atoms gradually shifted from the graphene plane are shown in Fig. 2. The sets of shifted atoms were chosen by adding layers of C-C bonds to a core consisting of a C atom or an aromatic ring. We defined the graphene patches such that the set of shifted atoms is surrounded by at least one layer of intact aromatic rings, to mimic the remaining planar graphene sheet. Shifting these atoms from the graphene plane elongates a certain number N of C-C bonds and simultaneously disturbs the same number N of aromatic rings. Dividing the difference obtained from a QM energy profile by N would give a combined energy of one C-C bond elongation and one aromatic ring disturbance, but separating the two components is impossible. Therefore, instead of trying to identify the energy corresponding to the elongation of an individual aromatic C-C bond, we considered the energy change of the whole atomic system as a reference to which we fit the MM energy profiles of the same system.

We used Gaussian09 for unrestricted calculations with the 6-31+G* basis set and the following methods: DFT (B3LYP,
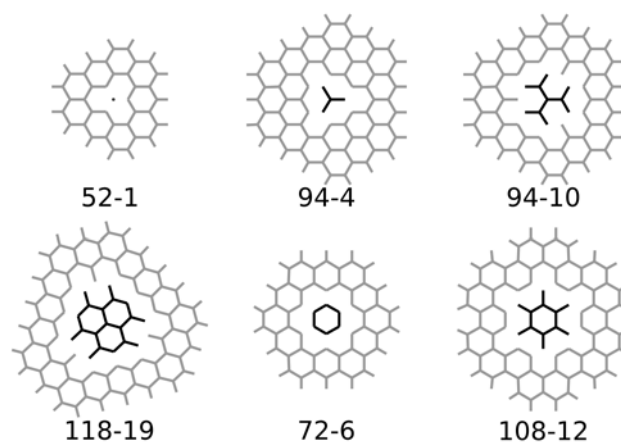
Fig. 2 Geometry of the graphene patches used for gradually shifting carbon atoms (black) out of the graphene plane (gray), identified by 2 numbers: the total number of atoms (including hydrogen atoms) and the number of carbon atoms shifted from the graphene plane. The sets of shifted atoms are defined by adding layers of carbon-carbon bonds to a core consisting of a carbon atom (52-1, 94-4, 94-10 and 118-19) or an aromatic ring (72-6 and 108-12).

BP86), hybrid (M06-2X, BHandHLYP) and self-consistent charge density functional tight binding (SCC-DFTB). With each method, we first ran an energy optimization for each graphene patch and then used the optimized structure as starting point for a rigid scan. To achieve a good precision of the QM energy profile, we chose a resolution of 0.001 nm for shifting the sets of atoms up to 0.01 nm from the plane, a resolution of 0.01 nm from 0.01 nm to 0.2 nm and a resolution of 0.02 nm from 0.2 nm to 0.5 nm, for a total of 45 single point calculations for each graphene patch. We note that for the 118-19 patch (Fig. 2), several single point B3LYP calculations did not converge; the energy decreased but continued to show small fluctuations. To minimize errors from missing points in the fitting procedure, we assigned to each point the lowest energy reached during the SCF calculation. Due to the small range of these energy fluctuations, using the average instead of the lowest energy would not affect the results. We used the least square method to fit the MM to QM energy profiles. We performed the MM potential energy evaluations used for parametrizing the Morse potential with GROMACS 4.5.3, with the parameters for aromatic carbons of the OPLS-AA force field[21] for the description of angles, proper and improper dihedral angles, and for the Lennard-Jones potential. No charges were assigned to atoms. Lennard-Jones interactions were calculated up to a 1 nm cut-off.

The fitting procedure starts from a random initial guess for D_{ij}, corresponding to which the r_c is computed as the inflection point of Eq. 1. As the bond is considered broken beyond the critical length and the potential is truncated, we fit MM po-
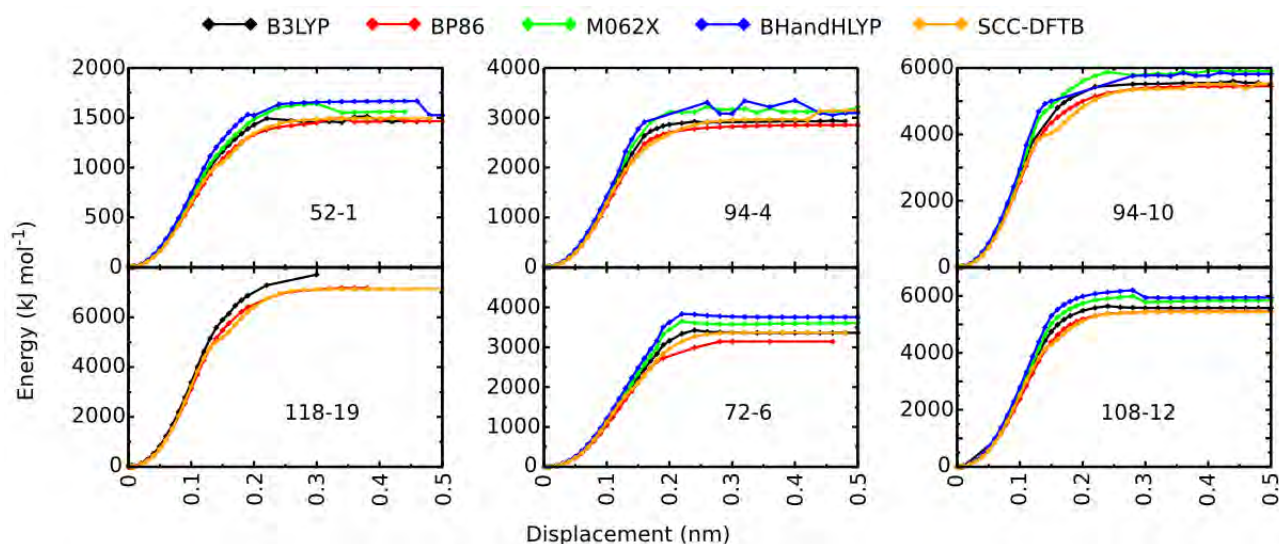
Fig. 3 Potential energy profiles for graphene patches from Fig. 2 for displacements up to 0.5 nm, comparing different QM methods. For the 118-19 patch, the M06-2X and BHandHLYP energy profiles could not be obtained due to unconverged calculations.

tential energies to the QM energy profiles only for the range of bond lengths between the equilibrium bond length, r_0, and the critical bond length, r_c. We approach the optimal D_{ij} during the fitting, and accordingly adjust r_c, i.e. fit to a different number of QM data points at each fitting step. The final D_{ij} defines the final critical bond length r_c. Consequently, the truncated Morse potential reproduces the increase in energy from zero to the inflection point.

We implemented the truncated Morse potential in GRO-MACS 4.5.3 by modifying the original Morse potential function. Although the potential function is continuous, retaining its value at r_c for bond lengths larger than r_c (Fig. 1), our implementation does not compute potential energy and force beyond r_c for efficiency, effectively setting both of them to zero.

For validation, we performed equilibrium MD simulations with this potential using GROMACS 4.5.3. We employed an integration time step of 1 fs and a 300 K velocity rescaling thermostat[22] with a time constant of 100 fs. For comparison, additional MD simulations using the AIREBO potential were performed with LAMMPS[23] version 17Feb2012 with an integration timestep of 0.5 fs, a 1.02 nm cut-off and including the Lennard-Jones and torsion terms. The computational efficiency was measured against the Tersoff and REBO potentials as well as ReaxFF with the same version of LAMMPS. For ReaxFF, we used the reax/c pair style with atom charges set to zero and charge equilibration disabled. Otherwise, parameters were identical to those described above for the energy evaluations.

3 Results

3.1 Parametrization

Fig. 3 shows the energy profiles obtained for the various graphene patches in Fig. 2. We observe a good agreement of the profiles obtained with different QM methods, suggesting our results to be overall robust with regard to the choice of the level of QM theory. We also note that the results from the computationally inexpensive SCC-DFTB method are often close to those obtained with the higher-level methods, in agreement with the findings of Cai *et al.*[24]. Although M06-2X is supposed to outperform B3LYP[25,26], we used the B3LYP energy profiles as reference for the MM fitting because they are the smoothest of the high-level methods and because M06-2X data for the 118-19 patch is missing. Furthermore, B3LYP is often used for parametrizing new compounds with the OPLS-AA force field[27,28]. For the rupture of benzene as a smaller reference system, B3LYP also compared favorably to higher level methods (MP2 and CCSD), which capture electron correlations and can be assumed to be more appropriate for systems with unpaired electrons, like those resulting from rupture of aromatic systems (see Fig. S1, ESI†). We applied the fitting procedure to the B3LYP potential energies shown in Fig. 3 for all six graphene patches from Fig. 2 independently.

Table 1 Dissociation energies D_{ij} for different graphene patches, using the B3LYP data as reference for MD fitting

Graphene patch	52-1	94-4	94-10	118-19	72-6	108-12
D_{ij} (kJ mol^{-1})	590	805	805	805	979	805

The resulting values for D_{ij} are listed in Table 1. We observed that the same value of 805 kJ mol^{-1} appears for four out of the six graphene patches and we therefore used this value in our force field. The corresponding critical bond length is 0.184 nm and the maximum force to which the bond can resist is 6285.6 kJ mol^{-1} nm^{-1}. We note that D_{ij} is only used as a bond-characteristic parameter in the fitting procedure, and therefore primarily reflects the slope in the potential up to the inflection point. Thus, D_{ij} should not be directly compared with the dissociation energy known for an aromatic bond. For the 52-1 and 72-6 patches we found D_{ij} values of 590 kJ mol^{-1} and 979 kJ mol^{-1}, respectively, *i.e.* values that are significantly different from the recurrent value of 805 kJ mol^{-1}. We hypothesise that the deviations result from differences in electronic conjugation, as electrons in these two specific subsets are not able to delocalize through conjugated double bonds after being shifted away from the graphene sheet. In the 52-1 patch there is no possibility of conjugation as only one atom is shifted, while in the 72-6 patch the benzene radical is a six-fold radical with none of the unpaired electrons being stabilized by conjugation. In contrast, in the other four cases, unpaired electrons at the outer carbon atoms are conjugated with the remaining delocalized π-system of the shifted subset of carbon atoms.

Fig. 4 shows an example of results from the fitting procedure for the 94-4 patch, with a D_{ij} of 805 kJ mol^{-1}. We obtained a very good agreement between the QM and MM energy profiles; the contribution from the Morse potential to the MM energy is significantly larger than the contributions from the other potentials, supporting our approach of using the original OPLS-AA potentials to describe most of the interactions while involving only the Morse potential in the fitting procedure. We note that the fitting was performed up to a displacement of 0.12 nm of the subset of atoms from the graphene patch, as at this distance the C-C bond length has reached the critical bond length of 0.184 nm.

3.2 Validation

3.2.1 Equilibrium bond lengths in graphene.
From QM energy optimizations, we found in the same graphene patch C-C bond lengths in the range 0.136 to 0.144 nm, while Reddy *et al.*[29] observed bonds ranging from 0.139 to 0.147 nm. In both cases, the graphene patches remained planar. Our truncated Morse potential uses an equilibrium C-C bond length of 0.14 nm to retain full compatibility with the original OPLS-AA parameters; from MM energy minimizations we also obtained planar structures. As expected, in an equilibrium MD simulation at 300 K, thermal motions of the atoms lead to fluctuations in bond lengths: in-plane motions can both lengthen and shorten the bonds, while out-of-plane motions can only lengthen the bonds. Fig. 5 shows the bond lengths distribution during the last 500 ps of a 1 ns simulation
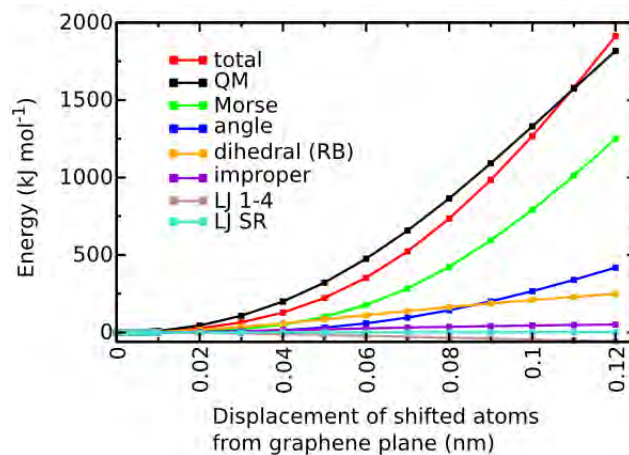
Fig. 4 Comparison between the potential energy profile obtained with B3LYP and the fitted MM force field using a truncated Morse potential with D_{ij}=805 kJ mol^{-1}, for the 94-4 graphene patch. The individual contributions to the MM potential energy are also shown. The displacements from the graphene plane correspond to bond lengths up to the critical bond length, and thus to those used in the fitting procedure.

with the truncated Morse potential. The average of 0.142 nm ($\pm$0.002) fits well within the range of values found from the QM calculations and is close to the average of 0.140 nm ($\pm$0.002) obtained from similar calculations using the computationally more expensive AIREBO potential. The critical bond length is significantly higher (by around 30%) than the average C-C bond length such that the probability of the critical bond length being reached, and therefore of bond break-
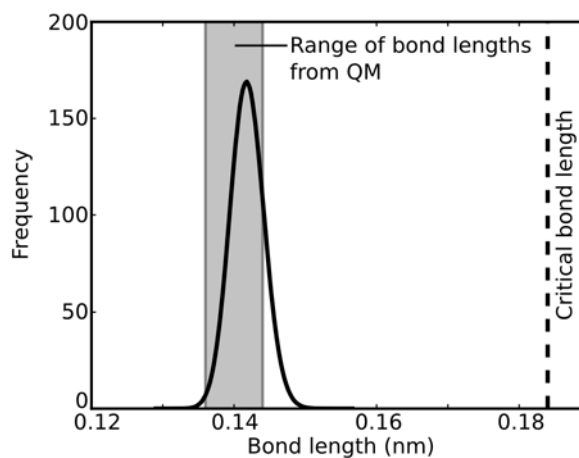
Fig. 5 Distribution of C-C bond lengths in an equilibrium MD simulation at 300 K using the truncated Morse potential. For comparison, the range of bond lengths observed in a B3LYP optimized graphene patch and the critical bond length corresponding to a D_{ij} of 805 kJ mol^{-1} are also shown.

Table 2 Wavelength and amplitude of ripples obtained from equilibrium MD simulations with the truncated Morse potential; averages and standard deviations (in parenthesis) are shown for cases where several simulations have been performed

Shape	Side or Radius (nm)	Atoms	Wavelength (nm)		Amplitude (nm)	
			armchair	zigzag	armchair	zigzag
square	100	394470	22.50	19.23	0.49	0.27
	50	99182	15.14	22.04	0.18	0.42
	20	16026	11.49	12.11	0.13	0.10
	10	4074	9.87	10.49	0.06	0.07
circle	100	1236250	18.60 (0.51)	19.69 (0.32)	0.28 (0.01)	0.24 (0.01)
	50	309658	15.88 (0.29)	17.55 (0.73)	0.19 (0.03)	0.20 (0.04)
	25	77710	13.88 (0.56)	15.12 (0.52)	0.13 (0.02)	0.13 (0.02)
	12.5	19594	10.71 (0.30)	11.52 (0.53)	0.09 (0.01)	0.08 (0.01)

ing, is practically zero in an equilibrium MD simulation. Only a significantly higher kinetic energy or applying mechanical stress could elongate the bond enough to break it. Furthermore, the maximum force to which the bond can resist is at least one order of magnitude larger than forces typically used for protein unfolding in pulling simulations[30,31], which is in line with the much higher mechanical stability of graphene as compared to proteins in atomic force microscopy experiments[32,33]. Thus, graphene sheets modeled with our truncated Morse potential can be used as substrates in biomolecular simulations.

3.2.2 Ripples in graphene during equilibrium MD. In experiments, free-standing graphene has been shown to spontaneously form ripples[34]. Using theoretical calculations, Fasolino *et al.*[35] and Abedpour *et al.*[36] suggested that they occur due to thermal fluctuations of the atoms, while Shenoy *et al.*[37] suggested that they are induced by edge stress in a whole nanoribbon due to its small width. Thompson-Flagg *et al.*[38] calculated a characteristic distance of penetration of ripples due to edge stress of 0.32 nm and held the presence of adsorbed OH (and possibly other) molecules responsible for the ripples throughout the sheets.

To study the vibrational behavior of graphene sheets modeled with our force field, we performed equilibrium MD simulations for finite sized sheets of shapes and dimensions listed in Table 2. We measured the amplitude and wavelength of the ripples in the graphene sheets by employing the one-dimensional FFT method described by Thompson-Flagg *et al.*[38] and averaging over the last 500 ps of 1 ns equilibrium MD simulations. For the circular graphene sheets we used a single line scan going through the center of the sheet in the horizontal direction (armchair orientation) or vertical direction (zigzag orientation). To estimate the variability of the results, we performed a series of 100 independent equilibrium MD simulations for the 25 nm circular graphene sheet.

We observed ripples appearing spontaneously throughout

the sheets in all simulations at 300 K, while the sheets remained planar when they were not coupled to a thermostat. Most of the sheets are significantly larger than the nanoribbons of Shenoy *et al.*[37] or the distance of penetration[38], so the rippling of the entire sheets cannot be induced exclusively by the edge stress. Thus, our results suggest that thermal fluctuations of the atoms can produce ripples as they were observed in experiments, thereby validating our model.

Meyer *et al.*[34] reported ripples with amplitudes of 0.2–2 nm and wavelengths of 2–20 nm from experiments. Theoretical calculations suggested amplitudes of 0.07 nm[35], 1 nm[38], or 0.21–0.28 nm (depending on armchair or zigzag orientation)[37] and wavelengths of around 8 nm[35], 9 nm[36], 10 nm[37], or 3–5 nm[38]. From simulations with the truncated Morse potential, we obtained the wavelengths and amplitudes listed in Table 2. From a smaller set of similar calculations with the more computationally expensive AIREBO potential we obtained the data listed in Table 3. We observed a general agreement of the results obtained with the truncated Morse potential with the ones obtained with the AIREBO potential and with the previous experimental and theoretical ones. Similar to Shenoy *et al.*[37], we also observed slight differences in the results for the armchair and zigzag orientations. More specifically, we found with both the truncated Morse and the AIREBO potential the wavelength in the zigzag orientation to be larger

Table 3 Wavelength and amplitude of ripples obtained from equilibrium MD simulations with the AIREBO potential on circular graphene patches

Radius (nm)	Atoms	Wavelength (nm)		Amplitude (nm)	
		armchair	zigzag	armchair	zigzag
50	309658	17.02	17.32	0.21	0.19
37.5	174472	18.62	11.64	0.22	0.60
25	77710	13.20	16.01	0.13	0.11
12.5	19594	11.17	13.21	0.08	0.07

Table 4 The 2D elastic modulus (E^{2D}), Young's modulus (E) and Poisson's ratio (v) obtained from MD simulations with the truncated Morse potential for armchair and zigzag orientations

Orientation	E^{2D} (N m^{-1})	E (GPa)	v
armchair	263.3	786.0	0.20
zigzag	276.7	826.0	0.17

than in the armchair orientation for most of the graphene samples. A dependency of the results on the size of the graphene sheet was also apparent. However, while we found the wavelength and amplitude to overall increase with sheet size as expected, exceptions do exist for both our truncated Morse and the AIREBO potential, and will be subject of future investigations.

3.2.3 In-plane Young's modulus and Poisson's ratio.
For further validation, we calculated Young's modulus (E) and Poisson's ratio (v) from MD simulations of square graphene sheets with a side length of 20 nm using our force field. We applied uniaxial tensional loads separately in the armchair and zigzag directions with a constant velocity of 10^{-3} nm ps^{-1} and a force constant of 10^5 kJ mol^{-1} nm^{-2}; the data from the last 500 ps of 1 ns simulations was used in elastic moduli calculations. We obtained the results listed in Table 4. As graphene is only one atom thick, elasticity was expressed by a 2D elastic modulus (E^{2D}, with units of force/length)[32] from which Young's modulus was derived considering a graphene sheet thickness of 0.335 nm; Poisson's ratio was computed from in-plane deformations. The values that we obtained for the elastic moduli and Poisson's ratios agree well with those measured by Lee *et al.*[32] and summarized by Scarpa *et al.*[39], respectively, further validating our model.

3.3 Computational efficiency

We compared our implementation of the truncated Morse potential in GROMACS and LAMMPS with the Tersoff[4], REBO[6], AIREBO[7], and ReaxFF[9] potentials as implemented in LAMMPS. The molecular system consisted of 19594 atoms in the shape of a 12.5 nm radius circular graphene sheet. The edge hydrogen atoms were removed when using the Tersoff potential, as parameters exist only for C, Si and Ge. For simulations of 100 ps running in parallel on 32 CPU cores, we recorded the running times shown in Table 5. The results show our potential to be almost twice faster than the fastest of the bond order potentials (Tersoff) and more than one order of magnitude faster than the slowest (ReaxFF). Such large differences were also independently reported for comparisons of different potentials in LAMMPS benchmarks[40]. When using our truncated Morse potential, the runtimes are nearly

halved in the more efficient GROMACS package as compared to LAMMPS.

The results emphasize the computational efficiency of a simple pairwise potential in comparison with the more complex bond-order ones. For each pair of atoms, the REBO and AIREBO potentials include a many-body term which reflects the position and chemical nature of neighboring atoms[7]. The difference between REBO and AIREBO consists in adding the Lennard-Jones and torsion terms[7]; they contribute to a better representation of the carbon based compounds, but seem to increase drastically the runtime. ReaxFF is around two orders of magnitude faster than the semi-empirical PM3 method[9], but due to its complexity (93 parameters for describing only hydrocarbon systems[9]) it is significantly slower than any other molecular mechanics force field included in this study.

4   Conclusions

We introduce here a truncated Morse potential which is parametrized based on data obtained from QM calculations to represent bond breaking in graphene patches. The pairwise potential is computationally inexpensive and simple to implement in software packages used for biomolecular simulations, so that mixtures of graphene or CNTs and biomolecules can be modeled straightforwardly and efficiently.

The dissociation energy profiles obtained from SCC-DFTB calculations on graphene are similar to the ones obtained from much more computationally expensive methods. This confirms previous results[24] showing that the efficient SCC-DFTB method is suitable to treat these highly conjugated carbon systems.

Our fitting procedure, which keeps the C-C bond length and force constant fixed to the respective OPLS-AA parameters for compatibility, yields a dissociation energy of 805 kJ mol^{-1}, which reflects the steepness of the QM potential up to the inflection point at which the bond bears the maximum force. As a consequence, this value overestimates the typical dissociation energies of around 500 kJ mol^{-1} known for aromatic or other conjugated systems. A distinctive feature of our potential is its truncation at the inflection point, which corresponds to a bond length of 0.184 nm. This allows the realistic treatment of ruptured bonds, which are generally unlikely to reform in fractured graphene. Due to its pairwise nature, our potential is not well suited for simulations which involve bond reforming; if such a process is expected, bond order potentials should be used instead.

Results obtained from equilibrium MD simulations using the truncated Morse potential compare favorably with experimental and theoretical results. For equilibrium MD simulations at 300 K, the bond lengths fit well within the range of values obtained in QM calculations, while the probability

Table 5 Runtimes (rounded to full seconds) for 100 ps simulations of 12.5 nm radius graphene sheets running in parallel on 32 CPU cores, and the slowdown relative to the truncated Morse potential in LAMMPS

Potential	Truncated Morse (GROMACS)	Truncated Morse (LAMMPS)	Tersoff	REBO	AIREBO	ReaxFF
Time (s)	383	690	1228	1482	4976	24172
Slowdown	0.6	1	1.8	2.1	7.2	35

of bond breaking is practically zero, ensuring the integrity of graphene sheets.

As further validation, the Young's modulus and Poisson's ratio as well as the wavelength and amplitude of thermally induced ripples fit well within the range of values measured in experiments. In particular, our data on ripples shows a quantitative agreement with experiments as good as the widely used and more complex AIREBO potential. Additionally, we find the truncated Morse potential to estimate rupture forces of graphene sheets under a spherical indenter as accurately as AIREBO, as shown in Part II[41].

Finally, our truncated Morse potential implementation is many times faster than the more complex reactive potentials. We note that this gain in efficiency is due to neglecting bond order, and thus on the expense of the accuracy in describing the physics of graphene or CNTs.

Given the overall agreement of simulations using our potential with experiments and other theoretical data, we propose the truncated Morse potential as a valuable force field for MD simulations of multi-million atom carbon based compounds and/or for simulations involving both graphene and biomolecular components. Due to its computational efficiency, the truncated Morse potential allows MD simulations involving large systems to reach experimentally or biologically relevant time scales of microseconds or beyond. Importantly, our potential also allows elasticity and fracture studies to be carried out upon applying a tensile force. However, when it comes to rupture mechanisms or bond reformation, bond order potentials like AIREBO are the methods of choice, as the truncated Morse potential does not describe properly bonds beyond their critical length.

This renders our new potential a good compromise between the accurate but complex bond order potentials and the highly approximate harmonic bond potentials, and makes it suitable for large or mixed simulations.

5   Acknowledgments

References

1 F. Chen and N. J. Tao, *Accounts of Chemical Research*, 2009, **42**, 429–438.

2 L. A. Ponomarenko, F. Schedin, M. I. Katsnelson, R. Yang, E. W. Hill, K. S. Novoselov and A. K. Geim, *Science*, 2008, **320**, 356–358.

3 T. Belytschko, S. P. Xiao, G. C. Schatz and R. S. Ruoff, *Phys. Rev. B*, 2002, **65**, 235430.

4 J. Tersoff, *Phys. Rev. B*, 1992, **46**, 15546–15549.

5 D. W. Brenner, *Phys. Rev. B*, 1990, **42**, 9458–9471.

6 D. W. Brenner, O. A. Shenderova, J. A. Harrison, S. J. Stuart, B. Ni and S. B. Sinnott, *Journal of Physics: Condensed Matter*, 2002, **14**, 783.

7 S. Stuart, A. Tutein and J. Harrison, *Journal of Chemical Physics*, 2000, **112**, 6472–6486.

8 J. H. Los, L. M. Ghiringhelli, E. J. Meijer and A. Fasolino, *Phys. Rev. B*, 2005, **72**, 214102.

9 A. C. T. van Duin, S. Dasgupta, F. Lorant and W. A. Goddard, *The Journal of Physical Chemistry A*, 2001, **105**, 9396–9409.

10 K. D. Nielson, A. C. T. van Duin, J. Oxgaard, W.-Q. Deng and W. A. Goddard, *The Journal of Physical Chemistry A*, 2005, **109**, 493–499.

11 A. K. Geim, *Science*, 2009, **324**, 1530–1534.

12 W. Qin, X. Li, W.-W. Bian, X.-J. Fan and J.-Y. Qi, *Biomaterials*, 2010, **31**, 1007–1016.

13 R. R. Johnson, A. T. C. Johnson and M. L. Klein, *Nano Letters*, 2008, **8**, 69–75.

14 R. Parthasarathi, N. R. Tummala and A. Striolo, *The Journal of Physical Chemistry B*, 2012, **116**, 12769–12782.

15 B. Hess, C. Kutzner, D. van der Spoel and E. Lindahl, *Journal of Chemical Theory and Computation*, 2008, **4**, 435–447.

16 D. A. Case, T. E. Cheatham, T. Darden, H. Gohlke, R. Luo, K. M. Merz, A. Onufriev, C. Simmerling, B. Wang and R. J. Woods, *Journal of Computational Chemistry*, 2005, **26**, 1668–1688.

17 B. R. Brooks, C. L. Brooks, A. D. Mackerell, L. Nilsson, R. J. Petrella, B. Roux, Y. Won, G. Archontis, C. Bartels, S. Boresch, A. Caflisch, L. Caves, Q. Cui, A. R. Dinner, M. Feig, S. Fischer, J. Gao, M. Hodoscek, W. Im, K. Kuczera, T. Lazaridis, J. Ma, V. Ovchinnikov, E. Paci, R. W. Pastor, C. B. Post, J. Z. Pu, M. Schaefer, B. Tidor, R. M. Venable, H. L. Woodcock, X. Wu, W. Yang, D. M. York and M. Karplus, *Journal of Computational Chemistry*, 2009, **30**, 1545–1614.

18 D. van der Spoel, E. Lindahl, B. Hess, A. van Buuren, E. Apol, P. J. Meulenhoff, D. P. Tieleman, A. L. T. M. Sijbers, K. Feenstra, R. van Drunen and H. J. C. Berendsen, *GROMACS User Manual version 4.5.4*, 2010, p. 69.

19 P. Atkins and J. De Paula, *Physical Chemistry*, W.H. Freeman, 2002.

20 S. J. Blanksby and G. B. Ellison, *Accounts of Chemical Research*, 2003, **36**, 255–263.

21 W. L. Jorgensen, D. S. Maxwell and J. Tirado-Rives, *Journal of the American Chemical Society*, 1996, **118**, 11225–11236.

22 G. Bussi, D. Donadio and M. Parrinello, *Journal of Chemical Physics*, 2007, **126**, 014101.

23 S. Plimpton, *Journal of Computational Physics*, 1995, **117**, 1–19.

24 J. Cai, G. Li, C. Wang and Z. Xie, *Journal of Materials Science and Technology*, 2010, **26**, 614–618.

25 J. Jiang, Y. Wu, Z.-X. Wang and C. Wu, *Journal of Chemical Theory and Computation*, 2010, **6**, 1199–1209.

26 S. Grimme, *Wiley Interdisciplinary Reviews: Computational Molecular Science*, 2011, **1**, 211–228.

27 W. Damm, A. Frontera, J. Tirado-Rives and W. L. Jorgensen, *Journal of Computational Chemistry*, 1997, **18**, 1955–1970.

28 J. Tirado-Rives and W. L. Jorgensen, *Journal of Chemical Theory and Computation*, 2008, **4**, 297–306.

29 C. D. Reddy, S. Rajendran and K. M. Liew, *Nanotechnology*, 2006, **17**, 864.

30 M. Sotomayor and K. Schulten, *Science*, 2007, **316**, 1144–1148.

31 H. Grubmüller, B. Heymann and P. Tavan, *Science*, 1996, **271**, 997–999.

32 C. Lee, X. Wei, J. W. Kysar and J. Hone, *Science*, 2008, **321**, 385–388.

33 P. E. Marszalek, H. Lu, H. Li, M. Carrion-Vazquez, A. F. Oberhauser, K. Schulten and J. M. Fernandez, *Nature*, 1999, **402**, 100–103.

34 J. C. Meyer, A. K. Geim, M. I. Katsnelson, K. S. Novoselov, T. J. Booth and S. Roth, *Nature*, 2007, **446**, 60–63.

35 A. Fasolino, J. H. Los and M. I. Katsnelson, *Nat Mater*, 2007, **6**, 858–861.

36 N. Abedpour, M. Neek-Amal, R. Asgari, F. Shahbazi, N. Nafari and M. R. R. Tabar, *Phys. Rev. B*, 2007, **76**, 195407.

37 V. B. Shenoy, C. D. Reddy, A. Ramasubramaniam and Y. W. Zhang, *Phys. Rev. Lett.*, 2008, **101**, 245501.

38 R. C. Thompson-Flagg, M. J. B. Moura and M. Marder, *EPL (Europhysics Letters)*, 2009, **85**, 46002.

39 F. Scarpa, S. Adhikari and A. S. Phani, *Nanotechnology*, 2009, **20**, 065709.

40 http://lammps.sandia.gov/bench.html\#potentials.

41 B. I. Costescu and F. Gräter, *Physical Chemistry, Chemical Physics*, 2014, **99999**, 99999.

Physical Chemistry Chemical Physics Accepted Manuscript